The Successful Application of Ground Penetrating Radar to Image Trace Element-Rich and Trace Element-Poor Siliceous Sinters

Bridget Y. Lynne and Cheng Yii Sim

Institute of Earth Science and Engineering, University of Auckland, Auckland, New Zealand
b.lynne@auckland.ac.nz • c.sim@auckland.ac.nz

ABSTRACT

In the early stages of geothermal exploration, with the help of ground-truthing via outcrop or coring examination, Ground Penetrating Radar (GPR) has proven a successful technique in mapping the lateral and vertical extent of hot spring siliceous sinter deposits up to depths of 10 meters. Alkali chloride fluid is the fluid we seek for our geothermal power plants, making sinters important in geothermal exploration. Sinters are important as they provide evidence of sites where alkali chloride fluid discharged at the surface. They are preserved for thousands of years after hot spring flow discharge ceases. Sinter samples were collected from Opal Mound, and Steamboat Springs, USA, and from Pukemoremore and Horohoro, New Zealand. Samples were specifically chosen to represent the opal-A to opal-A/CT to opal-CT ± opal-C to quartz silica phase diagenetic sequence and to include both trace element-poor and trace element-rich sinters. GPR was conducted over the sample sites in order to test the suitability of GPR in imaging sinters with different silica phases, density and porosity values and trace element compositions. The GPR imaging revealed that despite the differences in these sinters they were capable of reflecting the emitted high-frequency electromagnetic wave to produce clear GPR profiles. We therefore conclude that GPR can be used for imaging all types of sinters. The new application of GPR to image sinters provides a technique whereby we can map the subsurface extent of a sinter and are no longer limited to outcrop examination. This provides us with new information on the volume of sinter present at any one site which can be directly related to the amount of fluid discharged in an area, as well as a tool that enables mapping buried sinters that could cap a blind geothermal resource.

1. Introduction

As geologists, in the initial stages of exploration we are limited to the examination of rock outcrops. However, often much of the bedrock is below the surface and inaccessible. One technique successfully used to image the shallow subsurface (< 50 m) of many geologic settings is Ground Penetrating Radar (GPR) as reported by Jol (2009). GPR imaging provides information on buried rock formations such as the identification of stratigraphic boundary depths and/or changes in rock properties such as density, porosity or mineralogy.

Siliceous sinters are hot spring rocks that form from discharging alkali chloride water, the water type we use in our geothermal power plants. As the hot spring water discharges it cools and precipitates silica which accumulates to form rocks referred to as siliceous sinters. Sinters remain at the surface and a potentially useable geothermal reservoir remains at depth, for thousands of years after hot spring discharge ceases. Therefore sinters provide us with a direct link to a geothermal reservoir and are important in the early phases of geothermal exploration.

Over time, sinters undergo a series of five silica phase diagenetic transformations from opal-A to opal-A/CT to opal-CT ± opal-C to quartz (Lynne et al., 2005, 2007). Accompanying sinter diagenesis are changes in physical properties where porosity decreases and density increases. At some geothermal sites the discharging fluid contains significant trace elements such as arsenic, antimony and mercury. Such elements precipitate at the time of sinter formation becoming incorporated into the sinter, resulting in a strongly-coloured deposit (Lynne et al., 2005, 2008).

We applied GPR to trace element-poor and trace element-rich sinters from four locations to determine if GPR could image both types of sinter. We extended the study to include sinters that represented each silica phase and this provided a selection of samples that revealed a range of density and porosity values. We also examined the suitability of GPR to map the lateral and vertical extent of sinters. This capability removes the limitation of outcrops. The ability to image surface and subsurface sinter deposits

allows the volume of a sinter to be calculated. As sinter can only form from discharging alkali chloride fluids, understanding the volume of sinter provides valuable information on the mass flow from the reservoir to the surface. Apart from our work, GPR has not been previously used in geothermal environments (Dougherty and Lynne, 2010, 2011).

2. Site Locations

The sinter deposits at Opal Mound, Utah, USA, primarily occur along the north-trending Opal Mound fault that defines the western boundary of the Roosevelt geothermal system (Fig. 1A). The Opal Mound fault served as a fluid conduit for multiple generations of fluid discharge and sinter formation (Moore and Nielson, 1994). Sinter dated at 1630 ± 90 years old consists of a brightly coloured opal-A to opal-CT sinter while sinter dated at 1920 ± 160 years consists of a white quartz sinter (Lynne et al. 2005).

Steamboat Springs is located approximately 5 km south of Reno, Nevada, on the eastern side of the Sierra Nevada Mountains within the Great Basin, USA (Fig. 1A). The thermal area covers ~ 10 km^2 and includes ancient sinter deposits. The Steamboat Springs area has been a site of intermittent faulting, volcanic and hydrothermal activity for the last three million years (Silberman et al., 1976). Extinct sinter terraces consist of white opal-A to opal-CT sinter and coloured quartz sinter. A cored sinter deposit recovered from this area revealed dates between 6283 ± 60 years

and $11,493 \pm 70$ years (Lynne et al., 2008) indicating prolonged discharge of alkali chloride hot springs.

Horohoro is located at about 15 kilometres southwest of Rotorua City (NZGA, 2009) in the Taupo Volcanic Zone, New Zealand (Fig. 1B). Currently sinter deposits in this area remain buried. Besides two relatively small hot springs that still deposit small amount of sinter, there are no other surface manifestations in the area (Waikato Regional Council).

The Pukemoremore sinter is located within the Orakeikorako-Te Kopia geothermal system which lies in the Taupo Volcanic Zone, situated 20 km northeast of Taupo and east of Paeroa Range (Fig. 1B). The Paeroa Fault is the dominant feature of the area with a 400 m scarp that strikes northeast along the western side of the Paeroa Range, bisecting the Orakeikorako, Te Kopia and Waikite thermal areas. A step fault on the downthrown northwest side and the upthrown southeast side of the Paeroa Fault scarp (Wood, 1994) opened a conduit for thermal fluids to discharge at the surface. Clark (1999) gave a detailed report on the geology and geothermal activity of the area.

3. Methods

3.1 Silica Phases

X-Ray Powder Diffraction (XRPD) is the principal technique used to determine the type of silica phase present, as well as to compare the degree of lattice order/disorder among samples. XRPD analysis of samples was undertaken with a Phillips diffraction goniometer fitted with a graphite monochromator. Acquisition is controlled by Sietronics (1993) VisXRD software, and subsequent processing achieved using Diffraction Technology Traces V6 software. The XRPD comprises a Phillips PW1130 high voltage (HV) generator fitted with a copper (Cu) anode X-ray tube; the PW1050/25 goniometer uses a PW 1752 curved graphite crystal monochromator and a PW1965 proportional detector. The goniometer has been modified for computer control by the fitting of a Sietronics Sieray 112 stepper motor and control unit. Dry, untreated samples were ground in a mortar and pestle and pressed into an aluminum holder and scanned at 0.6° 2Ø/min, with a step size of 0.01°, from 10 to 40 °2Ø, and operating conditions of 40 kV and 20 mA, using CuKα radiation ($\lambda\alpha1 = 1.54051$ Å ; $\lambda\alpha2 = 1.5443$ Å).

The Full Width at Half Maximum (FWHM) is a guide to the degree of lattice ordering or silica phase maturation within each phase (Lynne et al., 2005, 2007). Lattice ordering increases with maturation from opal-A to quartz and is reflected by a narrowing of the XRPD scattering broadband. Typical FWHM values for immature opal-A, opal-A/CT, paracrystalline opal-CT ± opal-C and crystalline quartz sinters are 8.0 °2Ө, 5.0 °2Ө, 2.0 °2Ө, and 0.2 °2Ө.

3.2 Trace Element Composition

Samples were analysed by X-ray Fluorescence (XRF) to determine their chemical composition. Individual layers were dissected from the bulk sample so that only one colour was analysed at a time. Each sample was crushed in a tungsten carbide grinder to produce 10g of powder, which was mixed thoroughly with 1 ml of polyvinylpyrrolidine (PVP) and methyl cellulose in water and ethanol. Samples were mechanically pressed to N15 tonnes/kg into 40
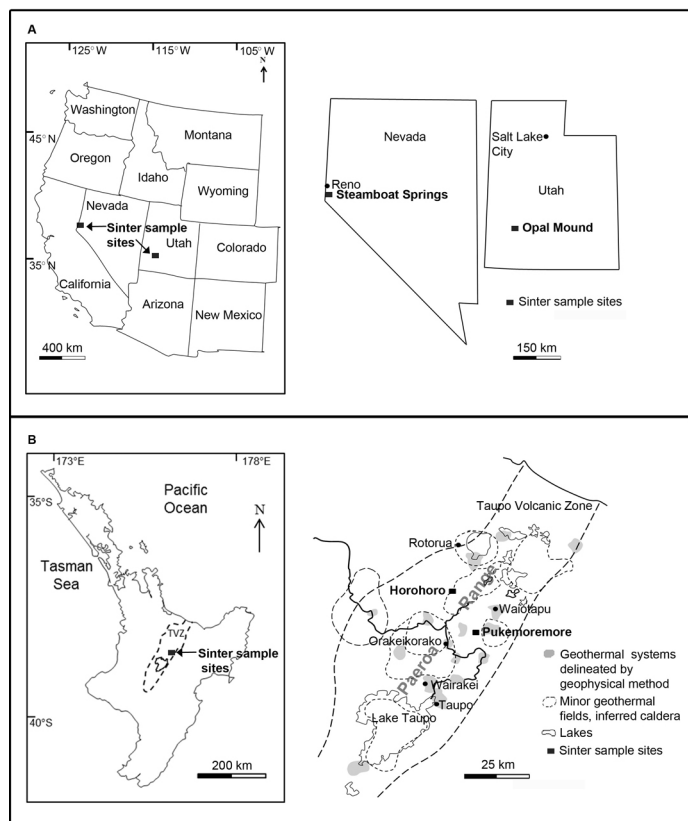
Figure 1. Maps of locations of sinter sample sites within the USA and New Zealand. (A) Map of Western USA on the left and locations of sinter sample sites in Nevada and Utah on the right. (B) Map of North Island, New Zealand on the left and locations of sinter sample sites in Horohoro and Pukemoremore on the right.

mm wide circular moulds. Once removed from the mould, samples were oven dried overnight. A Siemens SRS 3000 sequential X-ray spectrometer with a Rh tube was used to make a semi-quantitative analyses, and the results calibrated for all elements using three multi-element glass beads and a graphite disk. Brucker Spectra-plus (ver. 1.51) software was used to reduce the data.

3.3 Ground Penetrating Radar

Sinter outcrops were imaged using Ground Penetrating Radar (GPR). We used a GSSI (Geophysical Survey System Inc., USA) SIR-2000 GPR system with a transmitting antenna of 200 MHz center frequency. Both 200MHz and 400 MHz frequencies were used with variable settings to determine the best acquisition parameters at each site. The range settings varied from 100 to 300 nanoseconds depending on individual features and depth to attenuation. All transect lines were run at least twice, once with lowest possible frequency setting to penetrate the entire sequence to depth of signal attenuation and then again at highest frequency setting to acquire greater detail in the shallower subsurface. GPR data processing and analysis were performed using RADAN 6.5 Software. While more advanced processing such as running FIR (Finite Impulse Response) filter, bandpass filters as well as migration and deconvolution can be performed to reduce noises, it was decided that the minimally processed data be presented. Surface elevation data were collected using a Sokkia Electronic Total Station. Topographic corrections, normalization, stacking and depth conversions were achieved using the appropriate steps embedded in RADAN. After running several trials using different dielectric constants, a dielectric constant of 6 was used in siliceous sinter environments (Dougherty and Lynne, 2010) to convert travel-time to depth. The imaged depth shown in GPR signals was confirmed using cored samples. The geophysical records were ground-truthed to determine the nature of each reflection and the intermittent sedimentary layers using a vibracore or pulse-auger coring system and outcrop mapping of scarp exposures where possible. To ground-truth our GPR images, samples were collected in the field and their mineralogical and physical properties were established using XRPD analysis, XRF and density and porosity measurements.

4. Results

20 samples of trace element-poor and 16 samples of trace element-rich sinters from a total of 4 sites (Fig. 1) were chosen for GPR imaging. Sinter sites were chosen to cover the range of silica phases from opal-A to quartz (Figs. 2 to 8). These samples display variable density and porosity values but in general the density increases and the porosity decreases with silica phase maturation for trace element-poor sinters. Trace element-rich sinters show an increase in density with silica phase maturation but with minimal changes in porosity. These opal-A sinters are less

Table 1. Representative trace element-poor sinter samples for a range of silica phases from opal-A to quartz taken from four locations. A general increase in density and a decrease in porosity and FWHM value occur with silica maturation.

Trace Element Poor Sinters				
Sinter Phase	FWHM Value	Density (g/cm^3)	Porosity (%)	Location
Opal A	7.7	2.00	53	Horohoro, NZ
Opal A/CT	3.6	2.00	40	Pukemoremore, NZ
Opal CT	1.3	1.90	26	Steamboat Springs, US
Quartz	0.3	2.51	6	Opal Mound, US

Table 2. Representative trace element-rich sinter samples with different silica phases, ranging from opal-A to quartz taken from four locations. An increase in density, a decrease in FWHM value with a minimal change in porosity occurs with silica maturation.

Trace Element Rich Sinters				
Sinter Phase	FWHM Value	Density (g/ cm^3)	Porosity (%)	Location
Opal A	7.6	2.00	6	Opal Mound, US
Opal A/CT	4.0	2.10	6	Opal Mound, US
Opal CT	1.5	2.20	7	Opal Mound, US
Quartz	0.25	2.60	7	Steamboat Springs High Terrace, US

porous than trace element-poor opal-A sinters, therefore the porosity changes during diagenesis are less significant (Tables 1 and 2). Representative examples of each silica phase within the trace element-poor and trace element-rich categories are presented herein (Tables 1 and 2, Figs. 2 to 8). All GPR data was ground-truthed by coring or exposing buried outcrops. Sample sites are shown on each GPR image.
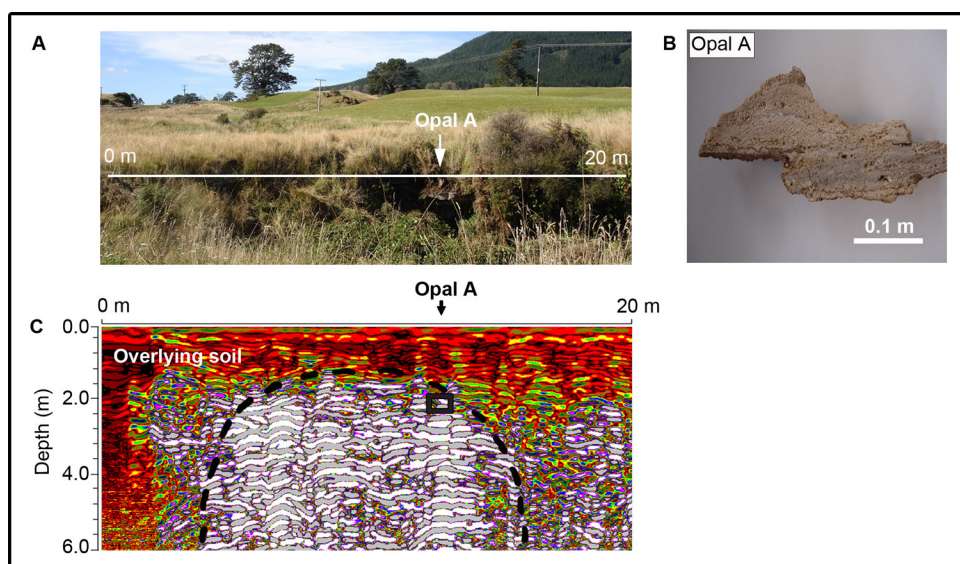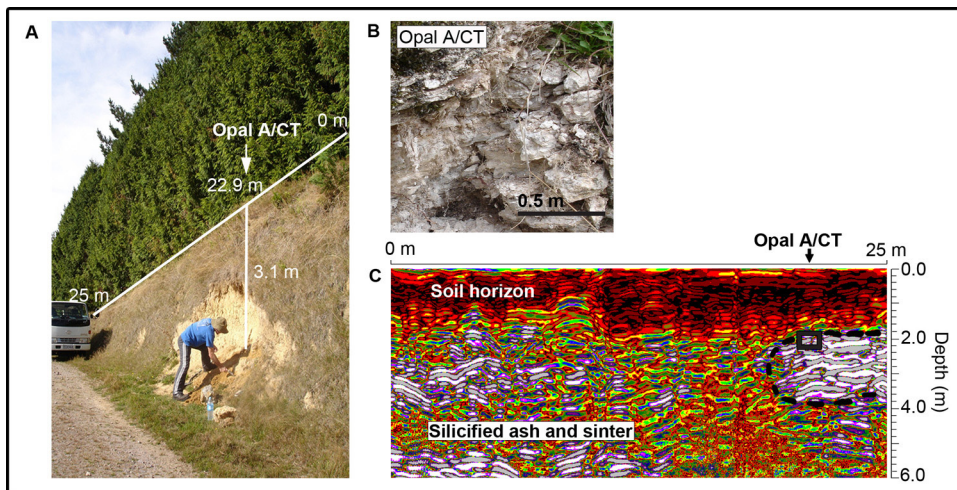

Figure 2. Trace element-poor sinter with opal-A silica phase and corresponding hand specimen and GPR image located at Horohoro, New Zealand. (A) Site photo of opal-A sinter outcrop and the 20 m GPR transect line which extends over the outcrop. Arrow showing the location of hand specimen collected. (B) Photograph of hand specimen of opal-A sinter sampled. (C) GPR image collected over outcrop. The grey and white coloured reflections indicate sinter at depth while the red and yellow reflections indicate overlying soil. The black box marks the location of the sinter sample collected and the dotted line shows the approximate boundary of the buried sinter (~12 m long x 4 m thick).
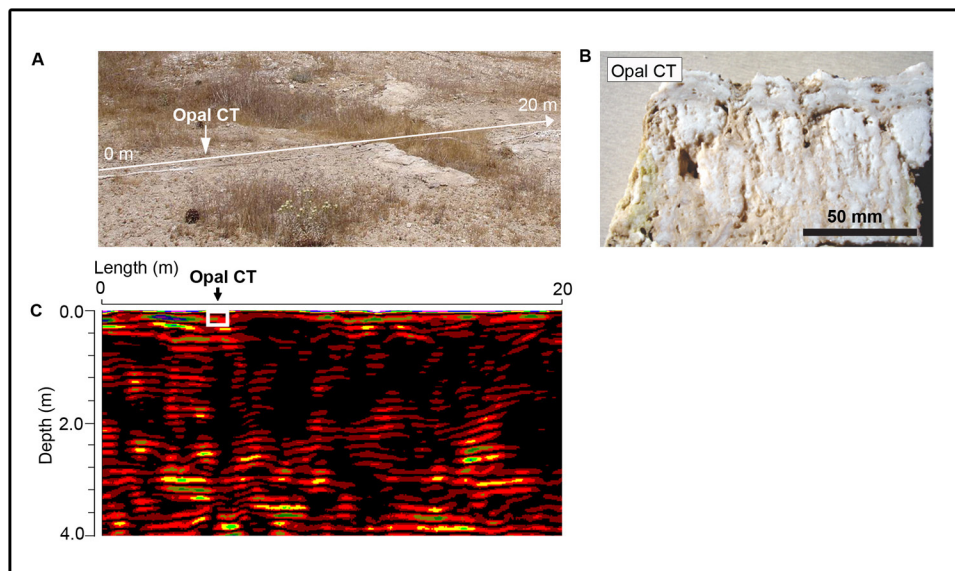
4.1 Trace Element-Poor Sinters

A sample representative of opal-A trace element-poor sinter was collected from Horohoro (Fig. 2A). A 1 m x 2 m sinter outcrop was visible within an overgrown and soil covered scarp. The sinter lies 1.8 m below the ground surface and the opal-A sample was collected from a depth of 2.3 m below the surface (Fig. 2B). The sinter has a FWHM value of 7.7 °2Θ, density of 2.0 g/cm³ and 53% of porosity. A GPR profile (Fig. 2C) was collected directly over the outcrop and extended for 20 m (Fig. 2A).

The GPR profile showed strong undulating reflections wherever the sinter occurred (grey and white areas on Fig. 2C). The strong reflections clearly define the subsurface boundary of the sinter (Fig. 2C dotted line around grey and white area) and shows how the sinter is far more extensive (estimated area = 12 m long x 4 m thick = 48 m²) than what is visually observed from the outcrop (~3 m²). The GPR image clearly defines the boundary between the soil cover (0 to ~1.8 m depth) and the buried sinter.

An opal-A/CT sinter sample was retrieved from a 0.5 m thick outcrop at Pukemoremore (Fig. 3A). This sinter revealed a FWHM value of 3.6 °2Θ, density of 2.0 g/cm³ and porosity of 40% (Fig. 3B). Our GPR profile over this outcrop showed strong reflections wherever the sinter was present (Fig. 3C). This outcrop was covered by 1.5 m of soil and the GPR clearly imaged the soil overlying the sinter. The lateral and vertical extent of the sinter is outline by the GPR image and can be
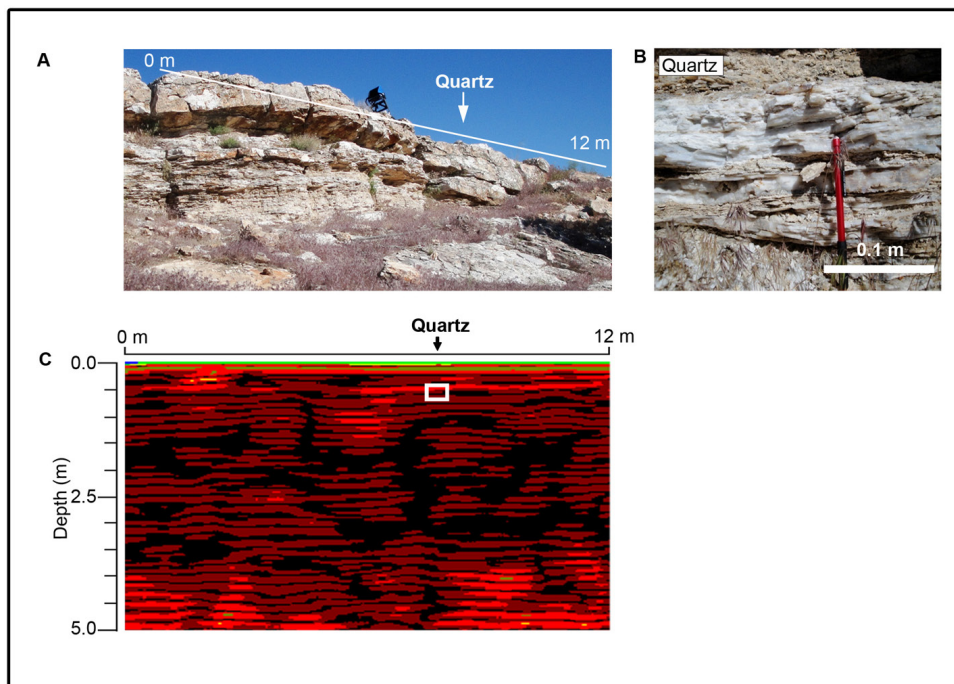

Figure 4. Trace element-poor opal-CT sinter collected from surface outcrop at Steamboat Springs, Nevada, USA. (A) Site photograph of opal-CT sample and the associated 20-meter GPR transect line collected. (B) Hand specimen of opal-CT. (C) Resulting GPR image. The GPR signals display the distribution of sinters (red areas) and fractures (black areas) at the subsurface. The white box marks the location of the sinter sample collected. The signals retrieved are weaker that those shown in Figure 2C and 3C as the GPR antenna used had a centre frequency of 200 MHz instead of 400MHz.

estimated at 2 m thick by 6 m long giving a total estimated area of 12 m² (Fig. 3C).

Opal-CT sinter was recovered from Steamboat Springs (Fig. 4A- 4B), and revealed a FWHM value of 1.3 °2Θ and density and porosity values of 1.9 g/cm³ and 26 % respectively. The sinter was exposed at the surface and covered an area of approximately 180 m². A GPR profile was collected over the sample site (Fig. 4A), revealing strong sub-horizontal reflections (brighter red areas on Fig. 4C) with multiple voids and subsurface fractures that often show interconnectivity at depth (black areas in Fig. 4C). At the uppermost surface, directly over the exposed sinter, the GPR image shows continuous strong reflections down to approximately 0.4 m depth and over the length of the 20 m GPR transect. This transect line was walked and sinter was confirmed at all locations along this GPR profile.

Quartz sinter collected from Opal Mound (Fig. 5A-5B) revealed a FWHM value of 0.3 °2Θ, density value of 2.5 g/cm³ and porosity value of 6 %. This sample was removed from a 2 m thick outcrop (Fig 5A). GPR successfully imaged the quartz sinter which is represented by the bright red reflections in the GPR profile (Fig. 5C). The GPR profile reveals almost horizontal bedding which is also visible in outcrop. A series of fractures visible in outcrop are shown as black areas in the GPR image. The GPR signals for opal-CT and quartz sinters taken from Steamboat Spring and Opal Mound (Figs 4-5) have

Figure 3. Trace element-poor opal-A/CT sinter with outcrop sample located at Pukemoremore, New Zealand and the corresponding GPR profile. (A) Site photograph of opal A/CT sample site with the 25 m GPR transect line along top of scarp. (B) Photograph of opal A/CT sinter outcrop. (C) Corresponding GPR profile. The distribution of the sinter is shown in the GPR image as grey and white reflections. The dotted line indicates the approximate boundary of the sinter (~2 m thick x 6 m long). The less reflective soil (red area) overlying the sinter is clearly shown in the GPR image. Silicified ash and inter-bedded sinter were identified south of the sinter outcrop and are shown here as mixed coloured, mainly grey and white, reflections.

Figure 5. Trace element-poor quartz sinter from an outcrop located at Opal Mound, Utah, USA. (A) Site photograph of quartz sinter outcrop and location of GPR transect line over outcrop. (B) Quartz outcrop. (C) GPR image of quartz sinter outcrop. The GPR image reveals strong reflections that correlate to the quartz sinter (red areas). The reflections are almost horizontal which can also be seen in outcrop as near-horizontal bedding planes. The black areas indicated subsurface fracturing and many of these fractures were also visible in outcrop.

weaker signals than those collected from New Zealand (Figs. 2-3) because the centre frequency of 200MHz was used in the USA while the 400MHz frequency was used in New Zealand.
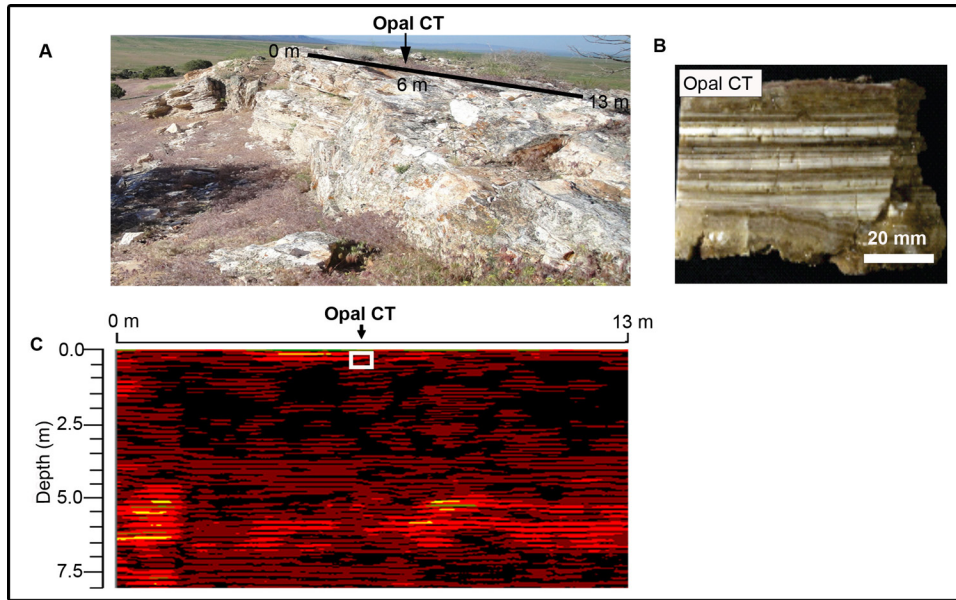
4.2 Trace Element-Rich Sinters

Strongly-coloured sinters from Opal Mound (opal-A, opal-A/CT and opal-CT) and mildly coloured quartz sinter from Steamboat Springs have been chosen to represent this group of sinters. At Opal Mound, the strongly coloured red and yellow in sinters are enriched in arsenic (1766 ± 2200 ppm), antimony (1649 ± 4730 ppm), aluminium (3067 ± 7870 ppm) and sulphate (2551 ± 5270 ppm). The red and yellow bands in sinters are caused by the presence of mercury and iron respectively. The brown opal-CT sinter is enriched in aluminium (~5000 ppm), calcium (~3500 ppm) and iron (~800 ppm). Pink colouration within the quartz sinter from Steamboat Springs is due to its mercury content (~1300 ppm).

Representative trace element-rich opal-A and opal-A/CT sinters outcrop were chosen from Opal Mound (Fig. 6A). The opal-A sinter shown in Figure 6B revealed a FWHM value of 7.6 °2Θ, density value of 2.0 g/cm^3 and porosity of 6%. The opal-
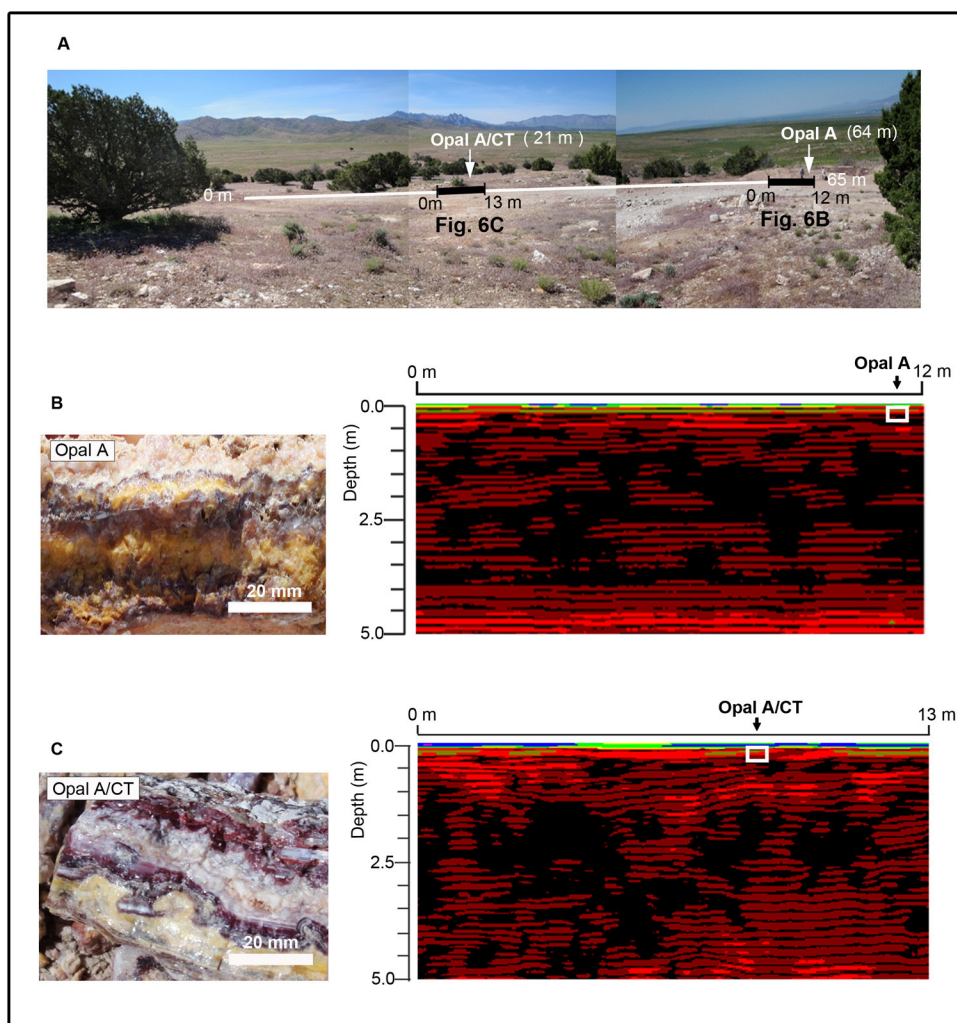
Figure 6. Trace element-rich opal-A and opal-A/CT sinters from Opal Mound, Utah, USA. (A) Photograph of the opal-A and opal-A/CT sinter sample sites and location and length of associated GPR transect lines taken along the main 65 m GPR transect line. (B) Opal-A sinter collected from the surface outcrop and associated GPR image showing the distribution of sinter (bright red areas) and fractures (black areas) within the subsurface. (C) Opal-A/CT sinter collected at the surface outcrop and associated GPR image reveals sub-horizontal strong reflections (red areas) that correlate to the near-horizontal bedding planes visible in hand specimen.
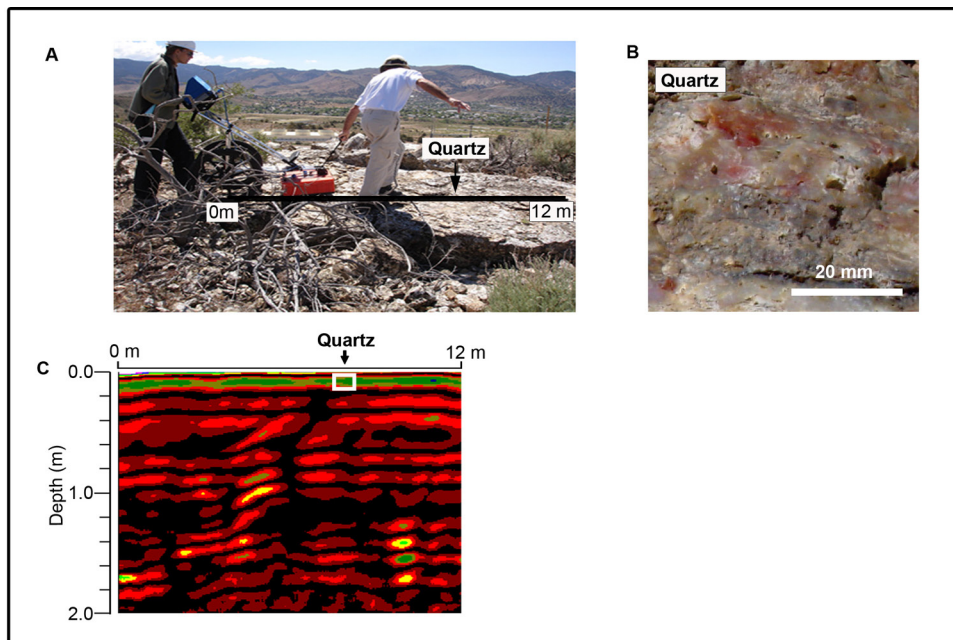
Figure 7. Trace element-rich opal-CT outcrop at Opal Mound, Utah, USA. (A) Site photograph of opal-CT sinter and the location of the 13 m GPR profile. (B) Hand specimen of opal-CT sinter. (C) GPR image, taken at where the sinter outcrops along the 13 m GPR transect line, shows strong continuous horizontal near-surface reflections (red areas) and the subsurface fractures are captured and shown as black areas.

A GPR transect line shows near-horizontal strong reflections (shown in red in Fig. 6B). These reflections correlate with the near-horizontal coloured banding shown in the hand specimen (Fig. 6B). Within the subsurface large cavities are revealed and may represent post-depositional fracturing of the sinter (black areas on Fig. 6B).

Figure 8. Trace element-rich quartz sinter collected from an outcrop at Steamboat Springs, Nevada, USA. (A) Site photograph of quartz and the associated GPR transect line across the sample site. (B) Hand specimen of quartz sinter. (C) GPR image displaying strong reflections associated with the quartz sinter (red areas). Fracturing is shown as black areas. The near-horizontal bedding visible in outcrop is also reflected by horizontal reflections in the GPR image.

The opal-A/CT sinter has a FWHM value of 4.0 °2Θ, density of 2.1 g/cm^3 and a porosity of 6 %. GPR was successful in imaging this sinter type (Fig. 6C) and revealed strong near-horizontal reflections over the opal-A/CT sinter (red reflections in Fig. 6C). The GPR profile shows similar subsurface fracturing (black areas in Fig. 6C) to that shown in the opal-A area (Fig. 6B).

Opal-CT sinter is represented by a 0.5 m thick outcrop (Fig. 7A) located at Opal Mound. This sinter has a FWHM value of 1.5 °2Θ and density of 2.1 g/cm^3 with a porosity value of 7 %. This strongly banded sinter of white, tan and brown reveals almost horizontal layering (Fig. 7B). The corresponding GPR trace (Fig. 7C) also revealed horizontal layering. Sinter was confirmed at the surface for the length of the GPR transect.

Quartz sinter from an outcrop 1 m thick located at Steamboat Springs represents this group of sinter (Fig. 8A). The quartz sinter (Fig. 8B) has a FWHM value of 0.25 °2Θ, and density and porosity values of 2.6 g/cm^3 and 7 % respectively. Strong, near-horizontal reflections were obtained by GPR imaging wherever the quartz sinter was located (Fig. 8C). The coloured areas shown in Figure 8C reveal the sinter has subsurface vertical fractures and laterally connected voids and/or fractures at depth (black areas on Fig. 8C).

4.3 Sinter Volume

One example where we imaged the extent of a buried sinter using GPR was at Horohoro, New Zealand (Fig. 2C). At Horohoro, a 2 m^2 area of sinter was observed in outcrop. However, by using GPR we were able to determine the lateral and vertical extent of the buried sinter to be at least 40 m^2. The use of GPR in sinter exploration work removes the restriction of only working with an outcrop and enables the volume of a sinter to be better estimated. For example at Opal Mound, Utah, USA a 1900 year old outcrop is exposed with dimensions of 15 m wide x 2 m thick (Fig. 9A) x 50 m long (Fig. 9B) which calculates to a volume of 1500 m^3. However, our GPR imaging revealed a large amount of sinter was buried. Based on the GPR profile and our ground-truthing, the volume of the sinter at this site was actually >50,000 m^3, an order of magnitude greater than estimated by outcrop. At this site there is a 36 MW geothermal power plant and no currently discharging hot springs. Estimating the
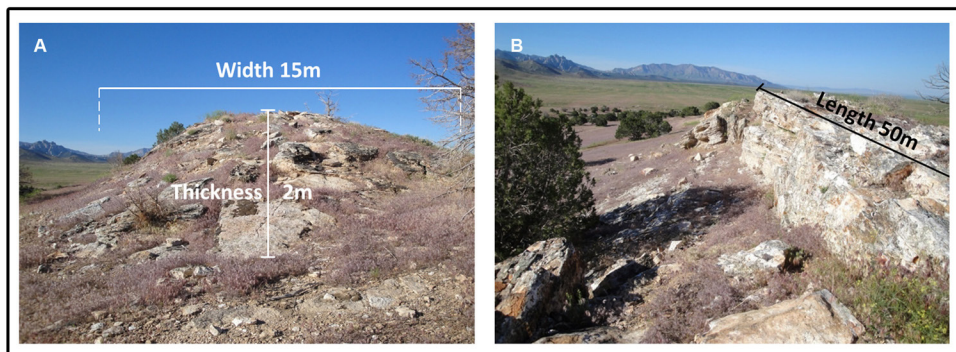
Figure 9. The 1900 year old sinter outcrop located at Opal Mound, Utah, USA, is exposed as 15 m wide x 50 m long x 2 m thick, resulting a volume of 1500 m^3. The GPR imaging however revealed a greater volume of buried sinter of >50,000 m^3 at this site. (A) Thickness and width of the exposed sinter outcrop. (B) Length of sinter outcrop.

volume of sinter at any geothermal site provides useful information as to the potential size of the geothermal resource.

5. Conclusion

The identification of siliceous sinters are important for early geothermal exploration as they form from discharging alkali chloride hot springs and provide evidence at the surface of a deeper potentially exploitable geothermal reservoir. Long after hot spring discharge ceases, sinters are preserved and the geothermal system may remain at depth. Therefore, sinters may be the only evidence at the surface of a hidden geothermal resource. The identification and mapping of preserved sinters reveals sites of former hot spring flow pathways. Ground Penetrating Radar (GPR) provides the ability to map the spatial extent of buried sinters removing the restriction of outcrop sampling providing a better understanding of the total mass flow of alkali chloride fluids discharged from any given geothermal area.

This study shows that GPR is a useful tool in imaging sinters regardless of silica phase, trace element composition, density or porosity. This simple technique can be added to and compliment other standard geological and geochemical work usually undertaken in the early stages of any geothermal exploration project.

References

Clark J.P., 1999. "Thermal evolution along the southern Paeroa Fault, between the Orakeikorako and Te Kopia geothermal areas, Taupo Volcanic Zone, New Zealand." Unpublised MSc., thesis, University of Auckland, p. 124.

Davis J.L., and A.P. Annan, 1989. "Ground-penetrating radar for high-resolution mapping of soil and rock stratigraphy." Geophysical Prospecting 37, p. 531-551.

Dougherty A.J., and B.Y. Lynne, 2010. "A novel geophysical approach to imaging sinter deposits and other subsurface geothermal features utilizing Ground Penetrating Radar." Geothermal Research Council *Transactions*, v. 34, p. 857-862.

Dougherty A.J., and B.Y. Lynne, 2011. "Utilizing Ground Penetrating Radar and Infrared Thermography to image vents and fractures in geothermal environments." Geothermal Research Council *Transactions*, v.35, p. 743-749.

Jol H.M., 2009. "Ground Penetrating Radar: Theory and Applications." Elsevier Science, p.544.

Lynne B.Y., K.A. Campbell, J.N. Moore, and P.R.L. Browne, 2005. "Diagenesis of 1900 -year old siliceous sinter (from opal-A to quartz) at Opal Mound, Roosevelt, Utah, U.S.A. Sedimentary Geology, v. 119, p. 249-278.

Lynne B.Y., K.A. Campbell, B. James, P.R.L. Browne, and J.N. Moore, 2007. "Tracking crystallinity in siliceous hot- spring deposits." American Journal of Science, v. 307, p.612-641.

Lynne B.Y., K.A. Campbell, J.N. Moore, and P.R.L. Browne, 2008. "Origin and evolution of the Steamboat Springs siliceous sinter deposit, Nevada, U.S.A." Sedimentary Geology, v. 210, p. 111-131.

Moore J.M., and D.L. Nielson, 1994. "An overview of the geology and geochemistry of the Roosevelt Hot Springs geothermal system, Utah." Utah Geological Association Publication 23, p. 25-36.

NZGA 2009, "New Zealand Geothermal Field" [online] available at: http://www.nzgeothermal.org.nz/nz_geo_fields.html#Horohoro.

Waikato Regional Council, "Geothermal Systems Map" [online] available at: http://www.waikatoregion.govt.nz/Environment/Natural-resources/Geothermal-resources/Geothermal-systems-map/Horohoro/.

Wood C.P., 1994. "Aspects of the geology of Waimangu, Waiotapu, Waikite and Reporoa Geothermal Systems, Taupo Volcanic Zone, New Zealand". Geothermics 23, p. 401-421.